Compact multichannel neutral particle analyzer for measurement of energetic charge-exchanged neutrals in Alcator C-Mod

V. Tang,[a] J. Liptac, R. R. Parker, P. T. Bonoli, C. L. Fiore, R. S. Granetz, J. H. Irby, Y. Lin, S. J. Wukitch, and The Alcator C-Mod Team
Plasma Science and Fusion Center, Massachusetts Institute of Technology, Cambridge, Massachusetts 02139

J. A. Frenje, R. Leiter, S. Mcduffee, and R. D. Petrasso
HEDP Group, Plasma Science and Fusion Center, Massachusetts Institute of Technology, Cambridge, Massachusetts 02139

(Received 8 May 2006; accepted 2 July 2006; published online 14 August 2006)

A four-channel compact neutral particle analyzer (CNPA) based on operating small Si diode detectors in pulse-height analysis (PHA) mode is used to measure energetic hydrogen minority ions with energies between ~50 and 350 keV stemming from ion-cyclotron range-of-frequency heated D(H) Alcator C-Mod plasmas with both active and passive charge exchange (CX). First core minority ion distribution results from Alcator C-Mod discharges and a detailed description of the diagnostic are presented. The diagnostic employs integrated electronics and fast digitization of the shaping amplifier voltage. The digitized data are stored for postshot PHA, which removes the constraints of real-time PHA and allows for improved performance via elimination of base line shift effects and potentially relieving pileup through Gaussian fitting routines. The CNPA is insensitive to the large gamma and neutron background in Alcator C-Mod discharges but is susceptible to the plasma's soft x-ray flux. The soft x-ray flux limits the CNPA energy resolution to ~15–20 keV. A simple model is used to interpret the active CNPA data which permits rapid estimates of the core hydrogen minority temperatures and anisotropy with a time resolution of ~100 ms. Hydrogenlike boron is identified as an important electron donor for the CX signal. © *2006 American Institute of Physics.* [DOI: 10.1063/1.2238519]

I. INTRODUCTION

Accurate velocity and spatial distribution measurements of ion-cyclotron range-of-frequencies (ICRFs) induced fast ions are important for verifying rf physics and heating deposition. Additionally, knowledge of the minority fast ion distributions is important for assessing their role in driving toroidal Alfvén eigenmodes and other Alfvén gap modes. Traditionally, a neutral particle analyzer is used to measure these fast ion distributions. Here, we present a Si diode-based neutral particle analyzer system for the Alcator C-Mod tokamak[1] ($R=0.68$ m, $a=0.22$ m, 8 T, and 2 MA) capable of diagnosing these energetic tails and compact enough to allow multiple channels with minimal port space.

Fundamental ICRF minority heating is the main auxiliary heating scheme on the Alcator C-Mod. Up to 5 MW of on-axis ($R=68$ cm) power can be deposited into bulk deuterium plasmas with hydrogen minority [i.e., D(H)] at 5.3 T and D(He_3) plasmas at 8 T, creating an anisotropic energetic minority distribution with energies up to ~300 keV.[2] Employing neutral particle analysis on Alcator C-Mod to measure these tails involves challenges such as limited diagnostic port space, high plasma densities ($n_{e0}\sim 10^{20}/\mathrm{m}^3$), and low signal-to-noise ratio. We are mainly concerned with D(H) plasmas, since analysis of D(He_3) discharges requires a difficult double-charge exchange.[3] The desire for multiple viewing chords with limited space prohibits the use of typical $E\|B$ neutral particle analyzers.[4] This difficulty compelled a unique multichannel Si diode solution with a direct view of the plasma and operated in postshot pulse-height analysis (PHA) mode using fast digitization techniques. This setup has the advantages of extreme compactness, lower equipment costs, and relative simplicity compared with traditional mass spectroscopy methods. For the 2005 Alcator C-Mod campaign, we implemented this four-channel compact neutral particle analyzer and operated it in both active [via a diagnostic neutral beam (DNB)] and passive neutral particle analyzer (NPA) modes. Similar diode-based NPA setups have been successfully employed on other fusion devices;[5,6] but none with Alcator C-Mod's high plasma densities and relatively weak neutral beam, and then only with real-time PHA. Instead of traditional real-time PHA, the compact neutral particle analyzer (CNPA) digitizes and stores the detector shaping amplifier voltage for postshot software analysis.[7] This arrangement eliminates base line shifts that can be significant during plasma events such as sawtooth crashes and allows for potential extraction of pileup pulses.

There are, however, some trade-offs in employing a Si diode system versus a normal neutral particle analyzer. First, without a steering electromagnetic field, the ability to diagnose different types of nuclei is lost. For Alcator C-Mod, this

[a]Author to whom correspondence should be addressed; electronic mail: vtang@mit.edu

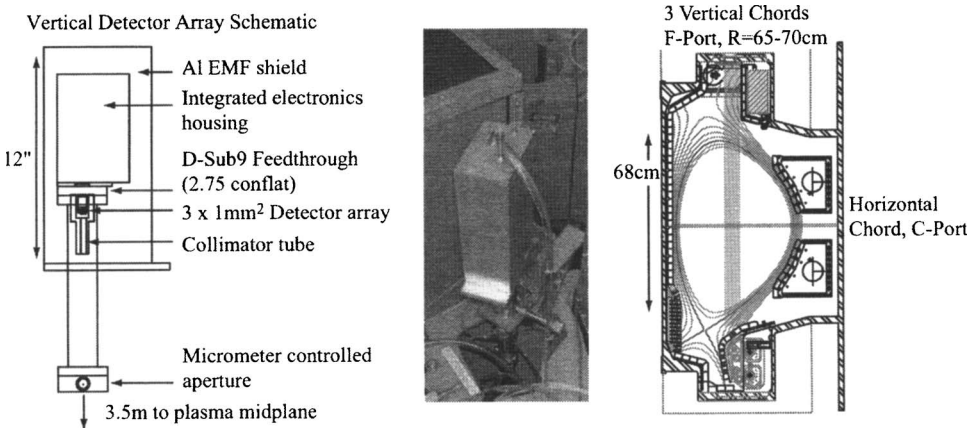

FIG. 1. Schematic of the three channel vertical detector array and the system sightlines in the plasma. The horizontal detector is mounted on a SMA feedthrough and uses a traditional NIM preamplifier with shaping amplifier setup. Its distance to the plasma axis is ~2 m.

is not an issue since only energetic hydrogen ions are created in ICRF heated D(H) plasmas, and the CNPA measures particles with energies greater than ~50 keV ($\gg T_{\text{bulk}}$ ~1–5 keV) only. Second, the direct-view diode system is susceptible to plasma soft x-ray noise, potentially more sensitive to cell emf pickup, and has a lower counting capability than an $E \| B$ analyzer. These constraints impose some limits on the operation of the CNPA and are considered.

In this article, we present the setup and operation of the CNPA diagnostic, calibration results, plasma background measurements, the postshot PHA routine, and initial temperature measurements of the hot ICRF minority tail on Alcator C-Mod. Modeling techniques required to extract minority tail distributions and rf deposition profiles from both active and passive measurements are also discussed. For these D(H) experiments, effective operation of the diagnostic is limited to low to moderate density ($n_{e0} < 2 \times 10^{20}/\text{m}^3$) Alcator C-Mod plasmas, due to penetrability of beam and signal neutrals.

II. DIAGNOSTIC SETUP AND DESCRIPTION

The CNPA consists of three vertical and one horizontal sightlines, as illustrated in Fig. 1. The sightlines of the diagnostic are arranged such that the three vertical chords view the phase space of the neutral distribution that is predicted to be most energetic, while the remaining horizontal channel sees neutrals that should be slower. The details of these sightlines and their detector systems are considered below.

The vertical viewing chords use a three channel, 3 $\times 1$ mm^2 IRD AXUV-3ELA detector array with a nominal 1500 Å thick Al foil for shielding visible light, while the horizontal channel utilizes an IRD AXUVHS5 subminiature (SMA) mount detector with a nominal 1000 Å Al foil. The actual foil thicknesses were inferred using an alpha source and the SRIM code.[8] The foils were found to be 1550 and 1250 Å thick, respectively. Hydrogen neutrals traversing the foil are assumed to be instantly ionized. The detectors are rated as 25 and 35 μm thick, have dead layers less than 70 Å, and were chosen to minimize response to the plasma neutron and gamma background. In addition to light shielding, the protective foils shelter the diodes from charge exchange (CX) neutral particles originating from the bulk plasma deuterium ions. The SRIM code predicts that the 1550 Å Al foil with an oxide layer is equivalent to a stopping power of ~14–21 keV for 50–350 keV hydrogen neutrals and ~12–17 keV for a 1250 Å Al foil. Consequently, the primary source of non-neutral noise for the diagnostic is the significant background plasma soft x rays (~1–10 keV) that are not blocked. This noise limits the resolution of the CNPA and typically the maximum permissible neutral count rate. This issue is analyzed in detail in Sec. IV. A variable knife-edge aperture determines the étendue of the vertical detectors, see Fig. 1. Normally, the vertical channels are operated with an étendue of $\sim 6 \times 10^{-12}$ m^2–sr. The vertical channels cover R from ~65 to 70 cm, depending on the aperture setting. Here we refer to them as Ch1 to Ch3, with Ch1 being the innermost channel and Ch3 the outermost. Typically, each diode in the array has a viewing cone width of ~2 cm at the midplane, and hence there is some overlap between the three channels. The horizontal channel, or Ch4, employs a permanent 6.3 cm long passivated stainless tube and pinhole (~0.25 mm D) for collimation. Its viewing cone width is ~3 cm on axis with an étendue similar to the vertical channels. Currently, the vertical channels view the radial injected DNB perpendicularly, while the horizontal channel is only available for passive CX experiments. With the DNB, there is some spatial localization of the CX signal for the vertical channels. All four channels essentially see particles with local $v_\parallel / v < \sim 5 \times 10^{-3}$. Thus, the vertical channels are geared toward observing particles with large $v_\perp$ at their banana tips. Again, the horizontal channel is designed to view a portion of the minority ion phase space that is weaker. This is discussed further in Sec. IV with Fokker-Planck simulations.

Electronically, the vertical detectors are connected directly to the integrated preamp lifier shaper amplifier housing via a D-sub9 vacuum feedthrough. The vertical channel array comes as an eight-pin dual in-line package (DIP) and is mounted on a Teflon socket with ~2.5 cm long, 30 gauge copper wire connections to the feedthrough. The integrated electronics housing contains three sets of ac-coupled Cremat CR-110 preamplifiers with 140 μs fall time connected to fixed gain Gaussian shaping amplifiers with a 1 μs pulse width and mounted on a primary motherboard. The amplifiers were developed in-house for the Alcator C-Mod hard x-ray (HXR) diagnostic.[9] Each set of preamplifiers/amplifiers is shielded from each other via an internal Al shield in the housing. This significantly reduced cross-talk between the channels to approximately 8%. The amplifier voltage outputs

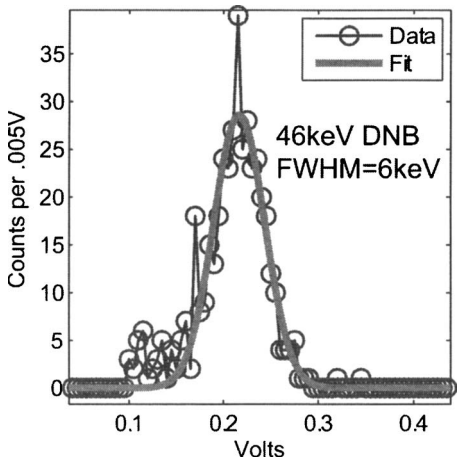

FIG. 2. Pulse-height spectrum from the vertical array for a beam-into-gas calibration with the DNB at 46 keV. The 46 keV DNB neutrals are slowed to ~24 keV by the CNPA protective foil. The FWHM of the DNB fit is ~6 keV and involves a convolution of the energy spread from the detector, the DNB, and the straggling through the Al foil.

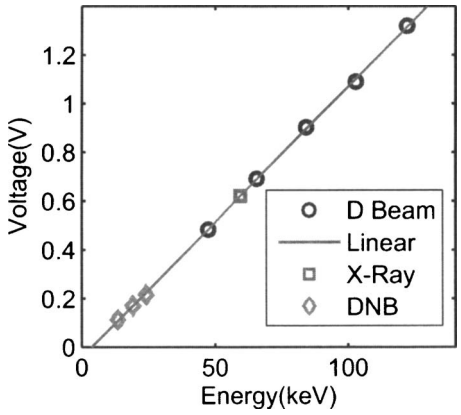

FIG. 3. Summary of the calibration data for Ch3 of the CNPA.

are then digitized at 10 Mhz by a D-tacq Dt216 compact peripheral component interconnect (CPCI) digitizer via 18 m of RG316 cables with SMA connectors. The electronic housing is an iridized Al enclosure and contains conducting gaskets for rf shielding; this box is placed within an additional Al rf shield that also covers the detectors. This Al shield eliminated emf noise and pickup from the equilibrium field (EF) coils and DNB due to typical machine operation, see Fig. 1. The operating range of the vertical channels is ~50–350 keV, limited by the shaping amplifier voltage rail, the attenuation of the Al foil, and the base line noise caused by the soft x-ray flux.

The horizontal channel uses a more typical nuclear instrument module (NIM) setup, with the detector ac coupled to an Ortec 142 preamplifier via a 7.6 cm long RG316 SMA cable. The Ortec preamp has a fall time of 44 μs. The use of preamps with fast fall times for the CNPA is critical as slower fall times allow the non-neutral signal to saturate the preamplifier quickly. An ~1 m long RG316 cable connects the preamplifier to an Ortec 572 shaping amplifier usually operated with a τ_s of 0.25 μs and a 100× gain, giving a base width of ~1.2 μs for each pulse. The amplifier voltage output is again digitized by a D-tacq Dt216 CPCI digitizer operated at 10 MHz and connected with 6 m of RG316 cable. emf noise and pickup are less of an issue for the horizontal channel because of its location. The electronics limit the horizontal channel to ~4 MeV for PHA for the above settings but because the amplifier parameters are easily changeable, different energy ranges can be chosen depending on expected plasma conditions.

The D-tacq Dt216 digitizer is the basis of the postshot PHA system. Enough memory is available on the digitizer for an entire Alcator C-Mod shot, typically around 2 s. These data, usually ~30–40 Mbytes, are then processed after the shot to extract pulse-height information. The removal of real-time processing constraints allows for sophisticated PHA software routines, such as fitting of pileup pulses. In addition, the full voltage data have been instrumental in discerning various electronic pickups, plasma induced noise, and preamplifier saturation for the CNPA. Currently, the CNPA is run at maximum count rates of $<100\,000/s$, which results in little pileup; hence, for simplicity and rapidness, the PHA routine currently employed does not perform Gaussian fits of each pulse. However, the routine does account for base line shifts and rejects the small amount of pileup that is present.

III. CALIBRATION AND PHA ROUTINE

The CNPA is calibrated with a combination of sources and the preamplifiers/motherboard's built-in test circuit. The vertical channels with fixed gains were calibrated with an Am^{241} 59.5 keV gamma source, a 60–140 keV deuterium ion beam operated by the PSFC HEDP group, and the Alcator C-Mod DNB at 33–46 keV during beam-into-gas experiments. The Rutherford backscattered flux from a thin gold foil is used with the deuterium beam to minimize potentially damaging fluxes to the detectors. The protective foil was not installed for the deuterium ion beam calibration. The beam-into-gas DNB data were taken with the protective Al foil in place; DNB neutrals at 33–46 keV are thus slowed to ~13–24 keV before they hit the detector. Additionally, the DNB calibration points are scaled by ~5%, based on known decreased detector efficiencies at these lower energies.[10]

Figures 2 and 3 show the calibration results for Ch3 of the vertical array using the above sources. The voltage to keV response for the channel is $V(E)=0.011E-0.043$. All three channels have slopes within ~5% of each other. In general the linear calibration fits are excellent. The total error in the calibration is estimated to be ~8%.

The horizontal CNPA channel is also calibrated with multiple sources; the Am^{241} gamma and alpha source, the preamplifier's test circuit, and the DNB at 46 keV. The ability to switch the voltage gain on the Ortec 572 shaping amplifier permits the use of the alpha source at 5.5 MeV without an attenuator. The horizontal channel voltage to keV calibration gives $V(E)=0.0026E+\pm 8\%$ for the settings described in Sec. II.

The PHA routine used for both calibration and plasma operation involves the following steps: (1) determine an average base line by smoothing the raw voltage base line data over a specific period, typically 0.1 ms, (2) subtract the voltage data with this smoothed base line, (3) find voltage peaks above a specified threshold, (4) reject pileup by considering

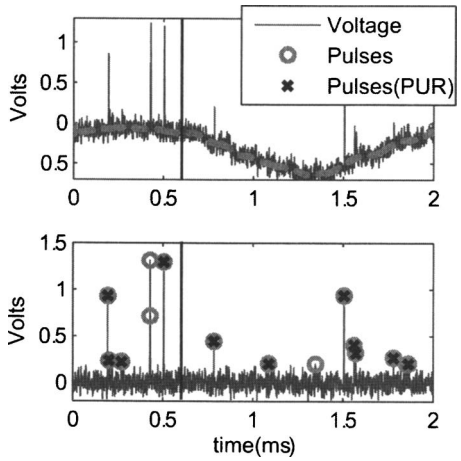

FIG. 4. PHA during a large sawtooth crash from shot 1050818008. The time axis in the plot is shifted for convenience. The first panel shows the shaping amplifier voltage from the horizontal channel during the crash, which occurs at $t \sim 0.6$ ms (vertical solid line). The soft x-ray flux from the central vertical chord goes from 90 to 60 kW/m^2 during this period. The base line shift is caused by the sudden burst of x rays and light of a large crash. The dash line is the base line used by the postshot PHA routine to correct for this large shift. The second panel shows the corrected voltage data with counts above 0.2 V marked by the PHA routine. Pulses (PUR) indicate counts that pass the pileup check.

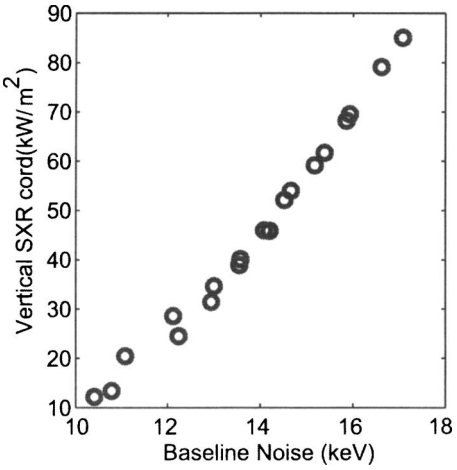

FIG. 5. Typical base line standard deviation as a function of soft x-ray flux for the vertical channels. The data shown are taken from the ramp-up phase of two low density *L*-mode discharges (1050818008 and 1050818011) before the application of rf.

the length of time between adjacent voltage peaks, and (5) find the peak of each pulse and store this value along with the time of the pulse. No fitting is used to determine the peak so there is a small tendency to underestimate the real peak value if the digitization rate is low compared with the pulse width. Figure 4 illustrates graphically some of these steps during a large sawtooth crash and clearly shows the importance of an accurate base line determination. The figure shows voltage data from the horizontal channel equipped with the Ortec 572 module which uses an automatic base line restoration circuit. Plainly, a traditional PHA approach would have missed counts with this skewed base line since the voltage threshold discriminator is constant, causing a false correlation with sawtooth crashes. The base line shifts in the vertical channels are significantly smaller. In general, it is likely that these shifts are related to the ac coupling time constants between each stage of the electronics and the sudden large rise in the detector base line current due to the sawtooth crash.

IV. OPERATING RESULTS

During the 2005 campaign, the CNPA was operated in both active and passive modes. In this section, we discuss the detectors' response to the plasma background, a simple model for interpreting CNPA data, spectra and minority distribution measurements from a low density *L*-mode shot, and the effect of residue neutral pressure to detector operation. First core minority ion distribution results from Alcator C-Mod discharges are presented.

A. Background response

The detectors are verified to have almost no response to the neutron and gamma background, allowing for operation in passive mode without background subtraction. The maximum neutron rate on C-Mod is typically $\sim 10^{14}$/s, resulting in only ~ 10 counts above 50 keV for the CNPA during a shot. The most significant non-neutral noise induced by the plasma is via soft x rays, which results in increasing fluctuations on the base line and limits the energy resolution of the detected neutral particles. These x rays have energies of $\sim 1-10$ keV, pass through the Al foil easily, and have mean free paths much less than the detector active thickness. The x rays also have the adverse effect of raising the energy threshold of detectable neutrals. Figure 5 is a plot of the base line noise level as a function of soft x-ray emittance for low density ($n_{e0} \sim 10^{20}/\mathrm{m}^3$), limited, *L*-mode shots that have a >70 keV passive CX neutral count rate of $\sim 10\,000$/s. Lower single null (LSN) shots typically have smaller soft x-ray emittance and thus permit higher count rates with the same resolution. This count rate/resolution trade-off can make it difficult to study transient fast ion events, such as fast ion diffusion from sawteeth. With low density plasmas, the DNB can increase the neutral signal by approximately an order of magnitude. These signal-to-noise ratio issues with the CNPA are probably unique to Alcator C-Mod, as other devices typically operate at much lower densities and employ strong heating neutral beams. Both of these differences can increase the fast neutral signal-to-noise ratio dramatically.

B. Spectra and inferred minority distributions

For CX, the line-integrated energy spectrum detected by the CNPA is given by[11]

$$F(E)dE = v^2 dv A\Omega \int_{-a}^{a} P(x,v) \times \left[\sum_s f_i(v,x)\sigma_{s,\mathrm{CX}}(v_{s,\mathrm{rel}})v_{s,\mathrm{rel}}n_s(x) \right] dx, \qquad (1)$$

where $F(E)dE$ is the number of particles with energy E through $E+dE$ hitting the detector per second, summed over contributions from different electron donor species s. a and $-a$ are the limits of the sightline. v is the minority hydrogen

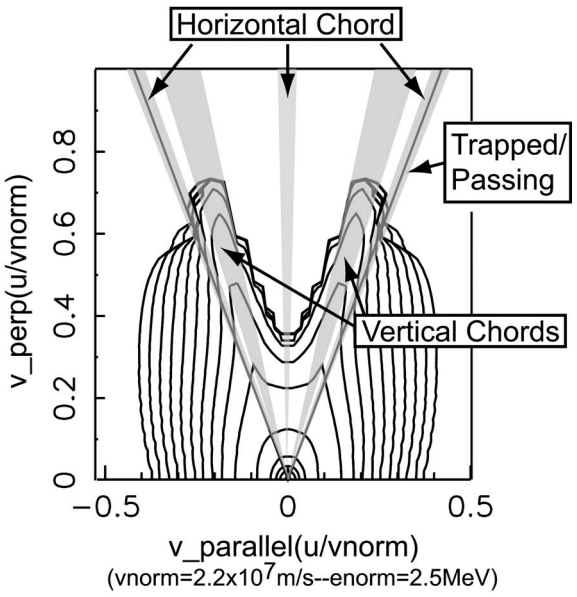

FIG. 6. Contour plot of minority hydrogen outboard midplane velocity at $r/a=0.23$ for a low density Alcator C-Mod shot from CQL3D simulations. The regions of the distribution viewed by the CNPA are qualitatively highlighted. The trapped/passing boundary is also indicated.

ion velocity, $f_i(v,x)$ the minority distribution, $\sigma_{\mathrm{CX}}(v_{\mathrm{rel}})$ the CX cross section based on the relative velocity of the minority ion and donor species, $P(x,v)$ the penetrability of the minority neutral hydrogen after CX out of the plasma, $A\Omega$ is the étendue, and $n_s(x)$ represents the density of the electron donor. Typically this donor is a neutral beam hydrogen (H^0) or residue deuterium neutral (D^0), but at hydrogen ion energies greater than ~100 keV CX with background hydrogenlike impurities can be important.[12] A delta function in velocity is assumed for the donor species. The pitch angle taken in f_i and $v_{s,\mathrm{rel}}$ is determined by the geometry of the sightline.

Based on Fokker-Planck solvers such as GENRAY/CQL3D (Ref. 13) and FPPRF,[14] energetic minority distributions in low density Alcator C-Mod plasmas are expected to be noticeably anisotropic in phase space. Figure 6 shows a CQL3D simulation of a limited *L*-mode low density Alcator C-Mod shot which clearly illustrates the anisotropy of the fast ion distribution at the outer midplane. The parts of the distribution viewed by the vertical and horizontal detectors are highlighted and show that the vertical channels should view the most energetic portions of the hydrogen distribution. These energetic "rabbit ears" in the outer midplane velocity distribution are a result of fast ion resonance localization,[15] which is characterized by energetic minority ions with banana tips near the resonant major radius. The vertical channels are thus designed to measure these minority ions at their turning point or banana tips, where the local $v_{\|}$ is ~0.

One rigorous method to interpreting CNPA data is to implement a synthetic diagnostic based on Eq. (1) in CQL3D. Because the DNB has a finite diameter [full width at half maximum (FWHM) ~12 cm] with spatial and phase space profiles, spatial localization of the CNPA signal using active analysis is not complete. Using a simulated diagnostic technique allows the spatial rf power deposition and temperature profiles to be inferred from the line-integrated active or passive CNPA measurements. In any case, for detailed power and temperature profiles, a synthetic diagnostic approach is required even for active neutral particle analysis. This work is currently ongoing.

C. A simple model

The simulated diagnostic approach is useful but time intensive. A much faster technique is used by several authors to infer an effective core minority distribution from NPA spectra.[12,16] After reviewing the model and discussing its assumptions, we extend and apply the method to a low density Alcator C-Mod shot and illustrate first experimental results from the CNPA.

The simple model assumes that the bulk of the hot minority tail is localized in the core($r/a<\sim 0.4$) of the plasma and that a relatively constant electron donor density from either the neutral background or a neutral beam is available for CX in that region. In the case of active analysis, there is some spatial localization depending on the FWHM of the DNB. Assuming further an isotropic distribution permits an estimate of the rf power deposition density through the Stix parameter.[17] Mathematically, for a detector with a radial sightline crossing the center of the plasma, these assumptions result in a sightline averaged core minority distribution given by

$$f_i(v) \sim \frac{F(E)}{\sum_s n_s \sigma_{s,\mathrm{CX}}(E_{s,\mathrm{rel}}) E_{s,\mathrm{rel}}^{1/2} E^{1/2} P(E)} \sim e^{-E/T_i}, \qquad (2)$$

where $P(E)$ is now the penetrability of minority hydrogen neutrals from the center of the plasma, $E_{s,\mathrm{rel}}$ the relative collision energy between the minority ions and electron donor species s, and E the energy of the minority hydrogen ion. Concerning the off-axis channels, derived distributions from sightlines not crossing the center of the plasma are weighted by different minor radii. T_i is an estimate of the minority temperature; it is an approximate peak minority temperature in the sightline if the fitted portion of the NPA spectra is greater than T_i, since the counts in those parts of the spectra are dominated by the hottest piece of the viewing chord.

The assumptions indicated for the simple model are not completely unjustified. In terms of the ICRF being core localized, Fokker-Planck and full-wave modeling results indeed predict that most of the rf power is absorbed within ~40% of the minor radius even for these low density plasmas. Concerning the neutral density profiles, the DNB does provide a roughly constant neutral hydrogen density in the core and some spatial core localization due to its finite FWHM width of ~12 cm. For passive analysis, the residual neutral hydrogen density is expected to vary $\pm\sim 50\%$ over an r/a range of 0–0.4 for an *L*-mode shot and, in exact contrast to the DNB, increase with r/a. Figure 7 illustrates the discussed assumptions and ideas graphically on a cross section of Alcator C-Mod.

Minority distributions from the CNPA vertical and horizontal channels calculated from this minimal model can reveal some details on how resonantly localized and anisotropic the minority hydrogen ions are. One simple comparison is to review the on-axis vertical data with the

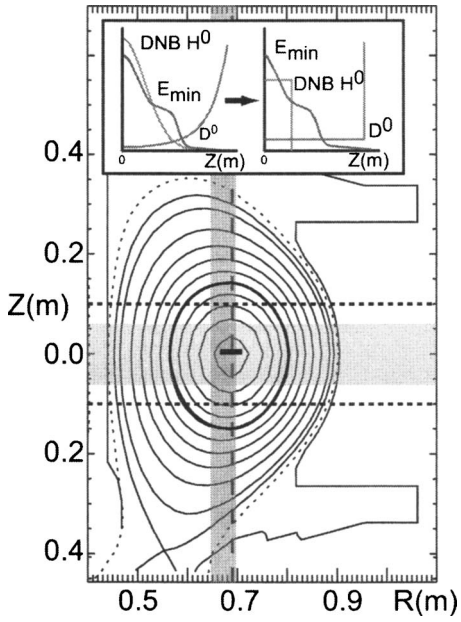

FIG. 7. LSN Alcator C-Mod discharge with ICRF, CNPA, and DNB overlays. The red vertical highlight indicates the CNPA vertical sightlines. The brown vertical dash line corresponds to the ICRF resonance layer of a typical 5.4T D(H) shot, with the small horizontal black line in the middle indicating the approximate width of the Doppler-broadened ICRF resonance for a hydrogen ion with $v_{\parallel} \sim 20$ keV. The green horizontal highlight shows the region up to the FWHM of the DNB, with the dashed horizontal black lines representing the 95% mark. The thickened flux surface marks the $r/a \sim 0.4$ point. On top, the left graph illustrates typical profiles of the DNB density, residue neutral deuterium density, and the averaged minority hydrogen energy. The right graph points out the approximations made by the simple model. Halo neutrals from the beam have a larger effective FWHM and make up about 1/3 of the beam induced signal.

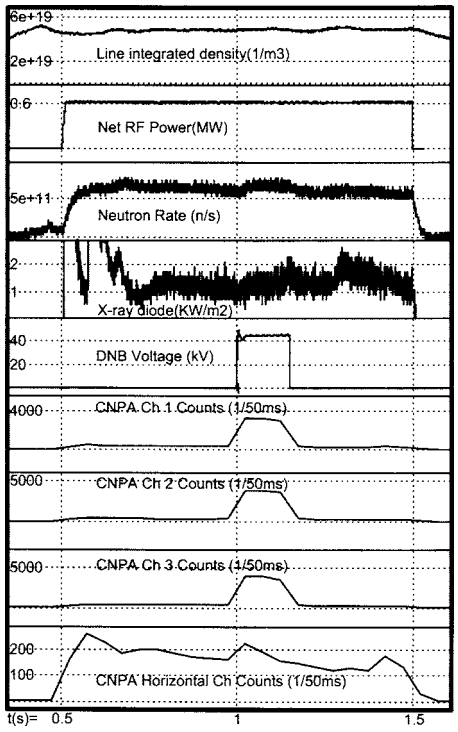

FIG. 8. Plasma parameters and CNPA count rates for shot 1051206002. The DNB fires from $t=1$ to 1.15 s. A large increase in count rate occurs for the channels viewing the beam. Fast particles are only detected when the rf is on.

horizontal channel measurements. If the distributions are completely isotropic, the calculated distributions from those channels should be the same since the measurements are weighted by approximately the same flux surfaces. The off-axis vertical channels are more difficult to interpret since they involve a move off both the plasma axis and resonance layer. These off-axis channels theoretically see no signal without collisions and Doppler broadening of the resonance since all the minority ions would otherwise have their banana tips right on the resonance layer. The effects of the broadening and collisions are indicated by the broadness of the rabbit ears and the degree of anisotropy in Fig. 6. The Doppler broadened resonance is typically several centimeters as indicated in Fig. 7 and spans the sightlines of the vertical channels for a typical Alcator C-Mod discharge. Assuming that the average temperature over the flux surfaces covered by the three vertical channels are roughly the same, the temperatures inferred form the off-axis vertical channels using the simple model then is a measure of the effective resonance layer width.

Overall, a model using the above approximations allows rapid estimates of minority tail temperatures and provides some information about the anisotropy of the minority ions.

D. Experimental data

Before applying the simple model to an Alcator C-Mod discharge, we must first uncover which electron donor species are relevant for CX in the energy range of the CNPA. Traditionally, only neutral beam and halo hydrogen were considered important, but, as stated above, fast ion CX with hydrogenlike impurities in the plasma can be an important neutralization process beyond ~100 keV for fast hydrogen minority ions. For Alcator C-Mod, the primary hydrogenlike impurity in the relevant energy range is B^{4+}, either from the small recombination population in passive analysis or from a larger equilibrium density sustained by beam charge exchange with fully stripped boron during active analysis. C^{5+} is also a possible contributor to the impurity CX but its cross section does not become significant until ~300 keV. Boron in Alcator C-Mod discharges stems from boronization and can result in B^{5+} densities of $\sim 1\%\ n_e$.[18] An approximate steady-state model for the core B^{4+} density neglecting radial transport is

$$n_{B^{4+}} n_e \langle \sigma v \rangle_e \Delta V_{\mathrm{tor}} = n_{B^{5+}} n_e \langle \sigma v \rangle_R \Delta V_{\mathrm{tor}} + \sum_s n_{B^{5+}} n_{\mathrm{H},s} \langle \sigma v \rangle_{\mathrm{CX}} \Delta V_{\mathrm{beam}}, \quad (3)$$

where the rate bracket subscripts, going from left to right, indicate electron impact ionization, recombination, and CX. The sum is taken over beam and halo components. V_{tor} refers to the flux tube volume at core of the plasma, and V_{beam} refers to the intersection volume between the DNB and that flux volume. For active analysis, the recombination term can be taken out via background subtraction. Analysis of this impurity CX show that for low density Alcator C-Mod shots, the CNPA spectra for active analysis up to ~200 keV are dominated by CX with beam and halo neutrals and from ~300 to 400 keV by B^{4+}. For passive analysis at 150 keV,

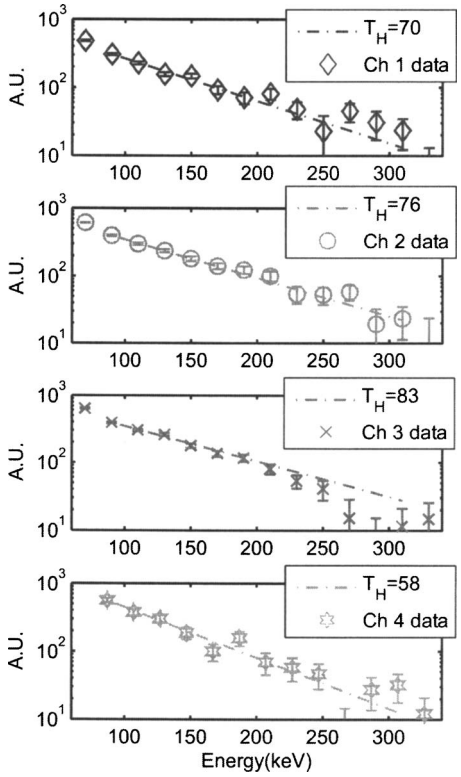

FIG. 9. The top three panels are active CX derived minority distributions, $f_i(v)$, from the vertical channels for shot 1051206002 using Eq. (2). The last panel plots the passive CX based distribution from the horizontal channel at t=0.85 to 1 s for the same shot. The error bars are derived from counting statistics only. A ±10% error is estimated for the fitted temperatures in the legends.

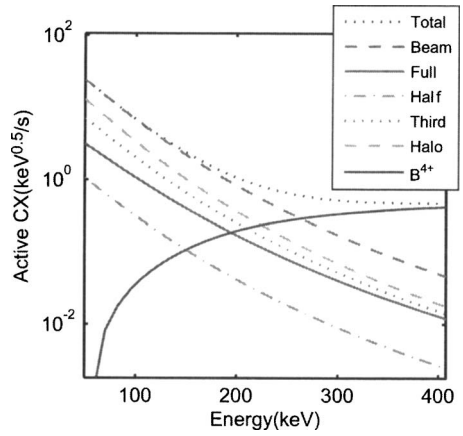

FIG. 10. $\Sigma_s n_s \sigma_{s,\mathrm{CX}}(E_{s,\mathrm{rel}}) E_{s,\mathrm{rel}}^{1/2} E^{1/2}$ from Eq. (2) for shot 1051206002 during active CX assuming a 1.5% boron impurity. The $E_{s,rel}^{1/2}$ factor has been converted to an equivalent proton velocity. The curves represent the probability that a fast proton will CX with a specific electron donor. Full, half, and third refer to the different components of the DNB. All DNB related electron donors are summed under beam. At energies lower than ~200 keV, the beam related donors are dominant.

the effective CX cross section is estimated to be ~20% higher than the cross section based on core neutral deuterium alone. This passive cross-section ratio increases rapidly pass 150 keV. Because of the lack of experimental cross sections for this fast proton-B^{4+} CX, theoretical cross sections are used for these calculations.[19]

Overall, concerning the quantities needed for Eq. (2) and their potential errors, active analysis should give the best distribution results. For active analysis, extensive data and comprehensive models are used to determine beam penetration and absolute beam densities in the plasma. Experimentally, spectroscopic measurements of the beam component fractions and FWHM measurements are available routinely for the Alcator C-Mod DNB. The beam penetration, beam densities, and halo density are modeled in detail using TRANSP (Ref. 20) and an in-house penetration code. These data and modeling produce accurate quantities for Eqs. (2) and (3). On the other hand, passive analysis is difficult since in a large part of the CNPA energy range absolute D^0 and B^{4+} densities are required to accurately interpret the CNPA spectra. The D^0 density is typically calculated from TRANSP, and the B^{4+} density can be calculated from Eq. (3) using B^{5+} densities inferred through spectroscopic measurements. For the penetrability factor in Eq. (2), fitted neutral stopping cross sections of Janev *et al.*[21] are used. For a shot with average $n_e \sim 8\times10^{19}/\mathrm{m}^3$, $T_e \sim 1.5$ keV, and a low edge gas pressure of ~0.1 mTorr, fast hydrogen neutrals from the center of Alcator C-Mod are attenuated by 30%–70% in the 50–350 keV range.

With the simple model defined for Alcator C-Mod, we now examine a low density, LSN, 5.4 T, 600 kA, ~7% n_H/n_e minority ICRF D(H) Alcator C-Mod shot, 1051206002, with this approximate approach. The transient plasma parameters, along with the count rates of the four CNPA channels, are shown in Fig. 8. The DNB fires from t =1 to 1.15 s, and the signal increase on the vertical channels are clearly seen. The slight rise in count rate for the horizontal channel is assumed to correspond to increased CX due to DNB produced B^{4+} ions streaming from the beam volume. Using the passive spectra from t=0.85 to 1 s for background subtraction, the DNB induced distribution data are illustrated in the first three plots of Fig. 9 along with temperature fits. The weighted Maxwellian fits using data from 90 to 320 keV for the peak temperature are ~70–80 keV for all three vertical channels. The errors in these temperatures are estimated by scanning the input parameters of the model and determined to be ±~10% for this discharge. Here, we use a fully stripped boron density of ~1.5% n_e, based on a core Z_{eff} estimate of ~1.25–1.75 inferred from visible bremsstrahlung and Thomson scattering data. For active analysis, the fit temperatures are weakly dependent on the boron density, even though the shape of the inferred distribution from 250 to 350 keV is not. This is discussed further below. For reference, the energies mentioned are the midpoints of 20 keV wide counting bins.

The passive CX based distribution and temperature fit for the horizontal channel are shown in the last plot of Fig. 9. For this data, we use a TRANSP based core neutral density of $10^{13}/m^3$ with the previous B^{5+} density of 1.5% n_e for Eq. (3). The inferred temperature is lower than the vertical channels estimates as expected from the Fokker-Planck modeling.

The relative effect of boron impurity CX is shown in Fig. 10 and illustrates the energy range where either beam neutrals or beam induced B^{4+} CX is dominant. A similar plot for passive CX is Fig. 11. Figure 12 plots for Ch2 during

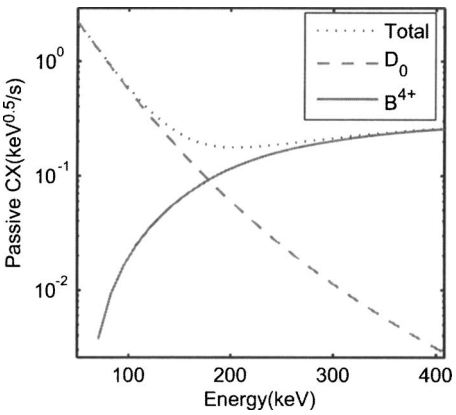

FIG. 11. $\Sigma_s n_s \sigma_{s,\mathrm{CX}}(E_{s,\mathrm{rel}}) E_{s,\mathrm{rel}}^{1/2} E^{1/2}$ from Eq. (2) for shot 1051206002 during passive CX assuming a 1.5% boron impurity. The $E_{s,\,rel}^{1/2}$ factor has been converted to an equivalent proton velocity. The curves represent the probability that a fast proton will CX with a specific electron donor. Passive boron CX becomes relevant at a much lower energy compared with active CX.

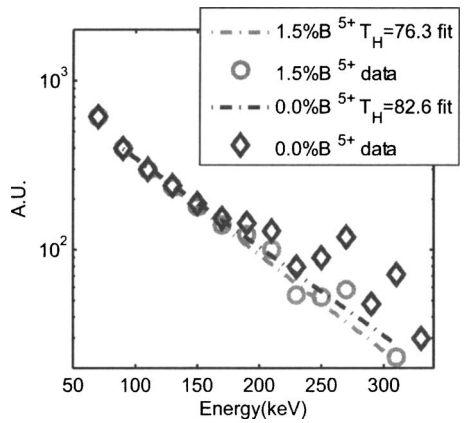

FIG. 12. Active CX derived minority distributions from Ch2 for different assumptions of the boron density. The peak temperatures deduced from Maxwellian fits are weakly dependent on the boron density, but the shape of the inferred distribution at energies greater than 200 keV is not.

active CX the deduced minority distribution spectra and associated weighted Maxwellian fit if impurity CX is neglected. As shown, the weighted Maxwellian fit employed for this shot is heavily biased by the beam dominated CX data points at lower energy, which have an order of magnitude higher number of counts. The difference between the peak temperature fits for analysis with and without boron is therefore only 6 keV. The overall fit itself is hence relatively independent of the small weighted contributions from the boron dominated CX energy range, while the slope of the distribution in that energy range is not. Additionally, the 1.5% B^{5+} fit seems to work well for the 175–300 keV energy range, where the CX has notable contributions from both hydrogen and boron. Hence, if the Maxwellian model is adequate, the CNPA can serve as an independent verification of the core boron impurity density. In summary, even if a measurement of the B^{5+} is not available, we can infer one to make the boron CX relevant parts of the CNPA spectra fit the Maxwellian distribution without affecting the overall minority tail temperature estimate very much. Work is continuing to verify these CNPA inferred boron densities from CXRS and Z_{eff} diagnostics.

E. Neutral-neutral attenuation

Finally, another significant effect that has to be dealt with is the attenuation of the CNPA signal via neutral-neutral and impact ionization collisions after the neutrals pass through the plasma. This is especially important for the vertical channels since they are ~3 m away from the plasma edge. Estimates and experimental results indicate that for edge pressures around 0.1 mTorr, this effect is ~20% for 50 keV particles but becomes a major factor at ~1 mTorr. Alcator C-Mod is unique in that most tokamaks operate with edge pressures much lower than ~1 mTorr, and thus edge attenuation is typically not a NPA issue.

ACKNOWLEDGMENTS

This work was supported by the U.S. Department of Energy, Cooperative Grant No. DE-FC02-99ER54512. The authors thank the diligence of the Alcator C-Mod science and technical staff.

[1] M. Greenwald *et al.*, Nucl. Fusion **45**, S109 (2005).
[2] P. O'Shea, Ph.D. thesis, Massachusetts Institute of Technology, 1997.
[3] G. W. Hammett, R. Kaita, and J. R. Wilson, Nucl. Fusion **28**, 11 (1988).
[4] R. Bartiromo, G. Bracco, M. Brusati, G. Grosso, S. Mantovni, B. Tilia, and V. Zanza, Rev. Sci. Instrum. **58**, 5 (1987).
[5] M. Osakabe *et al.*, Rev. Sci. Instrum. **72**, 1 (2001).
[6] K. Shinohara, D. S. Darrow, A. L. Roquemore, S. S. Medley, and F. E. Cecil, Rev. Sci. Instrum. **75**, 10 (2004).
[7] R. O'Connell, D. J. Den Hartog, C. B. Forest, and R. W. Harvey, Rev. Sci. Instrum. **74**, 3 (2001).
[8] J. F. Ziegler, J. P. Biersack, and U. Littmark, *The Stopping and Range of Ions in Matter* (Pergamon, New York, 2003).
[9] J. Liptac, R. R. Parker, V. Tang, Y. Peysson, and J. Decker, Rev. Sci. Instrum. (to be published).
[10] H. O. Funsten, S. M. Ritzau, R. W. Harper, and R. Korde, IEEE Trans. Nucl. Sci. **48**, 6 (2001).
[11] I. H. Hutchinson, *Principles of Plasma Diagnostics*, 2nd ed. (Cambridge University Press, Cambridge, 2002).
[12] A. A. Korotkov, A. Gondhalekar, and A. J. Stuart, Nucl. Fusion **37**, 1 (1997).
[13] R. W. Harvey and M. G. McCoy, The CQL3D Code, Proceedings of the IAEA Technical Conference on Advances in Simulation and Modeling of Thermonuclear Plasmas, Montreal, Canada, 1992 p. 527, available through UDSOC/NTIS No. DE93002962.
[14] G. W. Hammett, Ph.D. thesis, Princeton University, 1986.
[15] R. Kaita *et al.*, Nucl. Fusion **23**, 8 (1983).
[16] V. I. Afanassiev *et al.*, Plasma Phys. Controlled Fusion **39**, 1509 (1997).
[17] T. H. Stix, Nucl. Fusion **15**, 737 (1975).
[18] M. J. May, K. B. Fournier, J. A. Goetz, J. L. Terry, D. Pacella, M. Finkenthal, E. S. Marmar, and W. H. Goldstein, Plasma Phys. Controlled Fusion **41**, 45 (1999).
[19] T. G. Winter, Phys. Rev. A **35**, 9 (1987).
[20] D. McCune *et al.*, http://w3.pppl.gov/transp/
[21] R. K. Janev, C. D. Boley, and D. E. Post, Nucl. Fusion **29**, 2125 (1989).